

Hollow Nanospheres Organized by Ultra-Small $\text{CuFe}_2\text{O}_4/\text{C}$ Subunits with Efficient Photo-Fenton-Like Performance for Antibiotic Degradation and Cr(VI) Reduction

Dazhi Sun ¹, Jiayi Yang ¹, Feng Chen ², Zhe Chen ^{1,*} and Kangle Lv ^{3,*}

¹ School of Material Science and Technology, Jilin Institute of Chemical Technology, Jilin 132022, China; sundazhi@jlicet.edu.cn (D.S.); a4674360@sina.com (J.Y.)

² Jilin Petrochemical Company Organic Synthetic Plants, Jilin, 132021, China; chenfengcf666@163.com

³ College of Resources and Environmental Science, South-Central Minzu University, Wuhan 430074, China;

* Correspondence: chenazhe0809@foxmail.com (Z.C.); lvkangle@mail.scuec.edu.cn (K.L.)

Abstract: Hollow transition metal oxides have important applications in the degradation of organic pollutants by a photo-Fenton-like process. Herein, uniform, highly dispersible hollow $\text{CuFe}_2\text{O}_4/\text{C}$ nanospheres (denoted as CFO/C-PNSs) were prepared by a one-pot approach. Scanning electron microscope (SEM) and transmission electron microscope (TEM) images verified that the CFO/C-PNS catalyst mainly presents hollow nanosphere morphology with a diameter of 250 ± 30 nm. Surprisingly, the photodegradation test results revealed that CFO/C-PNSs had an excellent photocatalytic performance in the elimination of various organic contaminants under visible light through the efficient Fenton catalytic process. Due to the unique hollow structure formed by the assembly of ultra-small CFO/C subunits, the catalyst exposes more reaction sites, improving its photocatalytic activity. More importantly, the resulting magnetically separable CFO/C-PNSs exhibited excellent stability. Finally, the possible photocatalytic reaction mechanism of the CFO/C-PNSs was proposed, which enables us to have a clearer understanding of the photo-Fenton mechanism. Through a series of characterization and analysis of degradation behavior of CFO/C-PNS samples over antibiotic degradation and Cr(VI) reduction, $\bullet\text{OH}$ radicals generated from H_2O_2 decomposition played an essential role in enhancing the reaction efficiency. The present work offered a convenient method to fabricate hollow transition metal oxides, which provided impetus for further development in environmental and energy applications. **Highlights:** Novel hollow $\text{CuFe}_2\text{O}_4/\text{C}$ nanospheres were prepared by a facile and cost-effective method. $\text{CuFe}_2\text{O}_4/\text{C}$ exhibited excellent photo-Fenton-like performance for antibiotic degradation. Outstanding photocatalytic performance was attributed to the specific hollow cavity-porous structure. A possible mechanism for H_2O_2 activation over hollow $\text{CuFe}_2\text{O}_4/\text{C}$ nanospheres was detailed and discussed.

Keywords: hollow $\text{CuFe}_2\text{O}_4/\text{C}$ nanospheres; photo-Fenton; photodegradation of various pollutants; photocatalytic reaction mechanism

Citation: Sun, D.; Yang, J.; Chen, F.; Chen, Z.; Lv, K. Hollow Nanospheres Organized by Ultra-Small $\text{CuFe}_2\text{O}_4/\text{C}$ Subunits with Efficient Photo-Fenton-Like Performance for Antibiotic Degradation and Cr(VI) Reduction. *Catalysts* **2022**, *12*, 687. <https://doi.org/10.3390/10.3390/catal12070687>

Academic Editor(s): Natalia Martsi-novich

Received: 26 May 2022

Accepted: 20 June 2022

Published: 23 June 2022

Publisher's Note: MDPI stays neutral with regard to jurisdictional claims in published maps and institutional affiliations.



Copyright: © 2022 by the authors. Licensee MDPI, Basel, Switzerland. This article is an open access article distributed under the terms and conditions of the Creative Commons Attribution (CC BY) license (<http://creativecommons.org/licenses/by/4.0/>).

1.1 Chemicals and materials

All the reagents and chemicals Polyacrylic acid (PAA), Cupric chloride dihydrate ($\text{CuCl}_2 \cdot 2\text{H}_2\text{O}$), Ferrous chloride tetrahydrate ($\text{FeCl}_2 \cdot 4\text{H}_2\text{O}$), isopropanol (IPA) and aqueous ammonia solution ($\text{NH}_3 \cdot \text{H}_2\text{O}$) were purchased from Macklin biochemical technology Co. Ltd., China. They are analytical (AR) purity and used without further purified.

1.2. Experimental

1.2.1. Preparation of $\text{Fe}(\text{OH})_3/\text{PAA}-\text{Cu}(\text{OH})_2$ nanocomposites

For the preparation of $\text{Fe}(\text{OH})_3/\text{PAA}/\text{Cu}(\text{OH})_2$ nanocomposites, PAA solution (1 mL, $0.2 \text{ g} \cdot \text{mL}^{-1}$) and $\text{NH}_3 \cdot \text{H}_2\text{O}$ (1 mL, $2 \text{ mol} \cdot \text{L}^{-1}$) were added into 100 mL of deionized water for 40 min by stirring in a 1000 mL beaker. Then, 400 mL of IPA was added drop wise (1 drop/s) into the above solution under magnetic stirring. The 1.5 mmol $\text{FeCl}_2 \cdot 4\text{H}_2\text{O}$ was then added into the above solution with constant stirring for 180 min. Finally, the 0.75 mmol $\text{CuCl}_2 \cdot 2\text{H}_2\text{O}$ was added into the mixture for 12 h continuously in order to obtain a well-dispersed mixture. The $\text{Fe}(\text{OH})_3/\text{PAA}/\text{Cu}(\text{OH})_2$ was centrifuged and washed several times with deionized water and ethanol, and then dried at 400°C for 12 h. The obtained $\text{Fe}(\text{OH})_3/\text{PAA}/\text{Cu}(\text{OH})_2$ NSs were stored at room temperature for further experiments.

1.2.2. Preparation of CFO/C-PNSs.

The collected $\text{Fe}(\text{OH})_3/\text{PAA}/\text{Cu}(\text{OH})_2$ NSs was transferred into an alumina crucible and calcined, which was at 400°C with a heating rate of $2^\circ\text{C} \cdot \text{min}^{-1}$ and then maintained at 400°C for 2 h under N_2 atmosphere, which was denoted as CFO/C-PNSs.

1.2.3. Preparation of CFO -PNSs.

The procedure to fabricate CFO-PNSs was almost the same with CFO/C-PNSs, except that $\text{Fe}(\text{OH})_3/\text{PAA}/\text{Cu}(\text{OH})_2$ NSs was calcined in air atmosphere.

1.2. Material Characterization

The crystal structures of as-prepared composites were measured using X-ray diffraction (XRD, Rigaku D/Max-RB X-ray diffractometer) in the range of 5° – 90° . The morphologies of synthesized photocatalysts were determined by field emission scanning electron microscopy (FESEM, JEOL 7500F, Japan) and transmission electron microscope (TEM, JEM-2100F, JEOL, Japan). Ultraviolet/visible diffuse-reflectance spectra were recorded by using spectrophotometer (Lambda-750, PerkinElmer, USA) with BaSO_4 as a reference. The chemical states of elements were studied using an X-ray photoelectron spectroscopy (XPS) measurements. The Brunauer-Emmett-Teller (BET) surface areas of the samples were carried out via a nitrogen adsorption apparatus (ASAP 2020, Micromeritics, USA) and Barrett-Joyner-Halenda (BJH) method was used to study pore diameter distribution with adsorption data.

1.3. Photocatalytic degradation experiment

All the photocatalytic degradation experiments were carried out at room temperature, and the photocatalytic activity of different samples was also tested by the photodegradation of antibiotics, using a glass vessel with a water-cooling jacket as reactor (the temperature is about 15°C). Briefly, a certain amount of samples was dispersed into 30 mL of OTC (40 ppm), NFX (20 ppm), TCH (20 ppm), RhB (20 ppm), MO (40 ppm), Cr^{6+} (160 ppm) and aqueous solution. Before irradiation, the mixture solution was placed in darkness for 30 min to make the adsorption-desorption equilibrium between the contaminant solution and catalyst. The photo-Fenton experiments were carried out by adding a certain amount of H_2O_2 (200 μL , 35 vol.%), which was added into the above suspension and meanwhile was irradiated by a UV-Vis light (300 W Xe lamp). The vertical distance

between the mixture solution and lamp was about 12 cm. At a given time, 3 mL of the suspension was taken out and collected by centrifugation to remove the catalyst completely. The absorbance of antibiotic and industrial dyes solution was immediately analyzed by using a UV-vis spectrophotometer at the characteristic absorption peak. Every experiment was repeated at least twice. Typically, 18 mg CFO/C-PNSs photocatalyst with different scavengers were dispersed into 30 mL certain concentration contaminant aqueous solution, and the following processes were similar to the photodegradation process.

1.4. Active species trapping experiment and ESR measurements.

The free radicals capture tests were employed to study the mechanism for TCH degradation. Typically, 18 mg CFO/C-PNSs were dispersed into 30 mL of 20 ppm TCH aqueous solution with different scavengers. The active species were detected by adding isopropanol (IPA), triethanolamine (TEOA) and 4-hydroxy-TEMPO, which were respectively served as hydroxyl radicals ($\bullet\text{OH}$), hole (h^+) and superoxide radicals ($\bullet\text{O}_2^-$) quencher into the photocatalytic reaction systems, respectively. The processes were similar to the TCH photodegradation process.

Electron spin-resonance spectroscopy (ESR) was collected on a magnetech MS-5000 instrument. The ESR measurement with 5,5-dimethyl-1-pyrroline N-oxide (DMPO) as the spin trap was adopted to distinguish intermediate species especially such as superoxide anion radicals ($\bullet\text{O}_2^-$) generated during the reaction. Electron spin-resonance spectroscopy (ESR) for $\bullet\text{O}_2^-$ (superoxide radicals) was determined in dark and under visible light (methanol solution volume, 1.0 mL; sample, 3 mg; DMPO, 0.2 mL (1 M)).

1.5. Electrochemical measurements.

Electrochemical measurements were conducted through the electrochemical workstation (CHI760E, Shanghai Chen Hua Instrument Co., Ltd., China) by using a three-electrode system. The electrolyte was a 0.5 M Na_2SO_4 aqueous solution. The Ag/AgCl electrode, samples deposited fluoride-tin oxide (FTO) glass and Pt foil were served as reference electrode, the working electrode and counter electrode, respectively. The working photoelectrodes were prepared as follows: 30 mg catalyst was dispersed in 3 mL of ethanol and grounded for 8 min. Thereafter, the suspension was transferred onto a $1.2 \times 2.5 \text{ cm}^2$ FTO conductive glass by using a spin-coating method. Finally, the working electrode was obtained after dried at room temperature overnight.

The photocurrent response curves were obtained at 0 V with a 300 W Xe lamp irradiation. The electrochemical impedance spectroscopy (EIS) analyses were carried out at open circuit voltage in 0.1 M KCl solution containing 5 mM $\text{Fe}(\text{CN})_6^{3-/4-}$ with a frequency range from 0.01 Hz to 10 kHz. The linear sweep voltammetry (LSV) was recorded in the potential scanning ranging from 0.8 to -0.8 V under a 300 W Xe-lamp irradiation with sample interval of 0.001 V. The Mott-Schottky (M-S) data was recorded in the potential range from 0.8 to -0.8 V with a frequency of 1000 Hz.

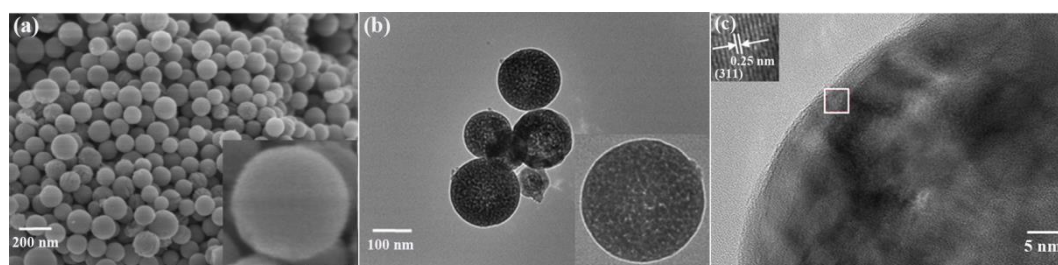


Figure S1. The SEM (a), TEM (b) and HRTEM (c) images for CFO-PNSs sample.

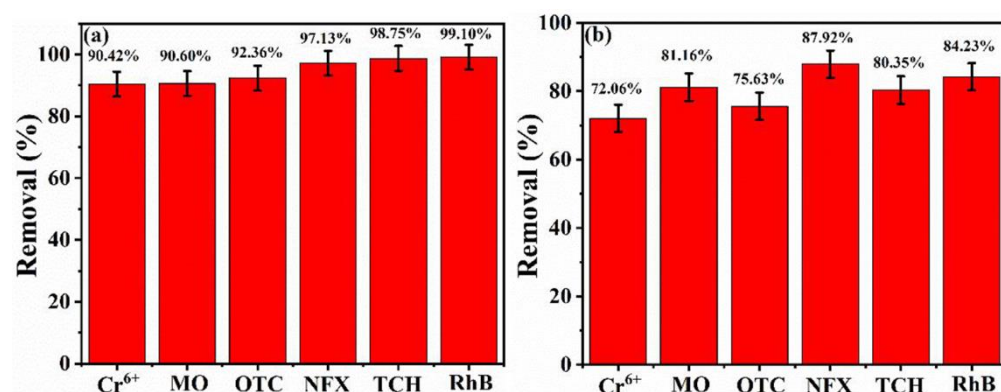


Figure S2. The removal rate of (a) CFO/C-PNSs and (b) CFO-PNSs for Cr^{6+} , MO, OTC, NFX, TCH and RhB.

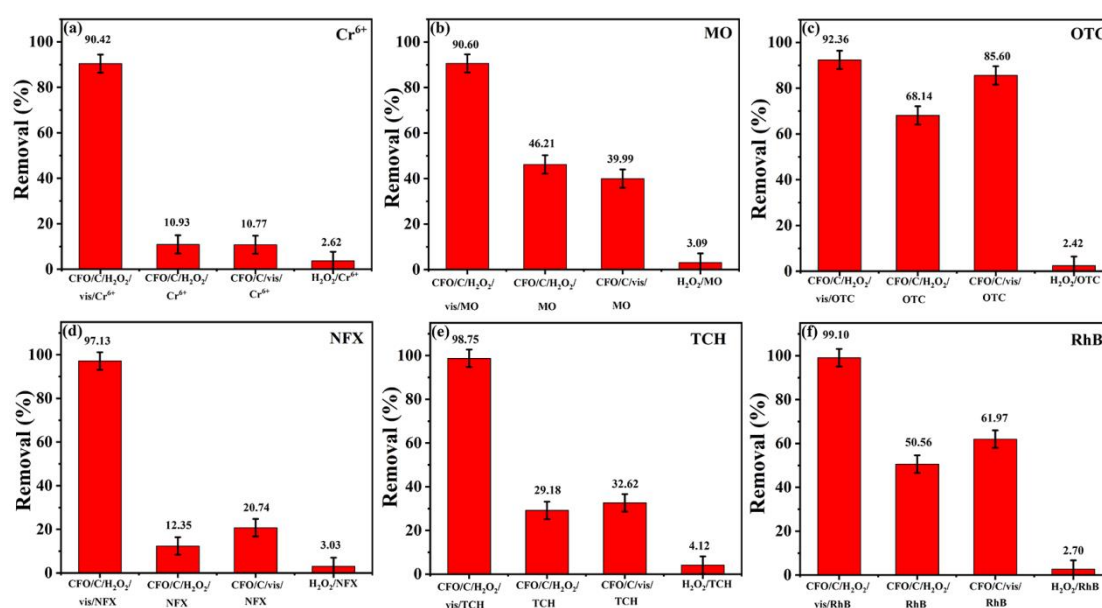


Figure S3. The photocatalytic degradation of (a) Cr^{6+} , (b) MO, (c) OTC, (d) NFX, (e) TCH and (f) RhB by CFO/C-PNSs with different conditions under visible light irradiation.

Table S1. The comparison of TCH photo-Fenton degradation activity of CFO/C-PNSs with previous literatures.

Photocatalyst	TCH Concentration ($\text{mg}\cdot\text{L}^{-1}$)	Dosage ($\text{g}\cdot\text{L}^{-1}$)	Time (min)	Removal (%)	Light source	Reference
ZnFe_2O_4 -10	60	0.3	40	98	LED lamp; $\lambda = 420 \text{ nm}$	1
$\alpha\text{-Fe}_2\text{O}_3/\text{g-C}_3\text{N}_4$ (Fe:C=1: 2)	10	1	150	90	300 W Xe-lamp	2
Fe^{2+}	100	0.005	60	94.2	4 W low pressure Hg UV lamps; $\lambda = 254 \text{ nm}$	3
CQDs/ $\alpha\text{-FeOOH}$ (CQDs 1 wt %)	20	0.25	60	94.5	350 W Xe-lamp; $\lambda > 420 \text{ nm}$	4
Fe-MOFs MIL-101	50	0.15	20	82.52	300 W Xe-lamp; $\lambda \geq 420 \text{ nm}$	5
$\text{g-C}_3\text{N}_4/\text{FeOCl}$ -20	50	0.1	60	90	300 W Xe-lamp; $\lambda = 400 \text{ nm}$	6
0.9% $\text{FeOOH}/$ - Bi_2WO_6	50	1	50	91	300 W metal halide lamp; $\lambda \leq 420 \text{ nm}$	7

Ag ₃ PO ₄ @MIL-53(Fe)M:A=10:1	10		60	95.18		8
10% α -Fe ₂ O ₃ /BiOI	20	1	30	82.1	Xe-lamp; $\lambda < 420$ nm	9
CuCo ₂ O ₄	50	0.2	5	89.1	400 W MW oven; T=90 °C	10
{110} facets Fe ₃ O ₄ NPs	50	0.3	60	96.7	10 W UVC-lamp; $\lambda = 220-275$ nm	11
0.1% CuS/Bi ₂ WO ₆	40	1	50	73	300 W metal halide lamp; $\lambda \geq 420$ nm	12
MnFe ₂ O ₄ /bio-char	40	0.5	120	95	300 W Xe-lamp; $\lambda \geq 420$ nm	13
(0.75:1.5) NiFe ₂ O ₄ /C	20	0.3	60	97.25	visible-light; ($\lambda > 400$ nm)	14
α -Fe ₂ O ₃ @TiO ₂	50	0.5	90	100	300W Xe-lamp; $\lambda > 420$ nm	15
Fe ₃ O ₄ @void@TiO ₂	40	0.25	6	100	300W Xe-lamp; $\lambda = 200-1000$ nm	16
CuFe ₂ O ₄ /C	20	0.6	60	98.75	300 W Xe-lamp; $\lambda \geq 400$ nm	This work

Table S2. The comparison of photo-Fenton degradation activity of CFO/C-PNSs with previous literatures.

Catalyst	Concentration (mg·L ⁻¹)	Dosage (g·L ⁻¹)	Time (min)	pollutant	Removal (%)	Light source	morphology	preparation methods	Reference
CuFe ₂ O ₄ /NC	15	0.3	90	Levofloxacin (LVFX)	84.87%	—	nanoparticle	solvothermal method	17
CuFe ₂ O ₄	20	0.16	150	Malachite Green (MG)	82.8%	300 W Xenon lamp	Porous and spongy	solution combustion synthesis	18
oxygen vacancies-CuFe ₂ O ₄	10	0.1	90	sulfamethazine (SMT)	95%	500 W Xenon lamp; $\lambda > 420$ nm	raw expanded perlite	precipitation-calcination method	19
CuFe ₂ O ₄ /AgBr	16.34	1.51	120	acid red 88 (AR88)	94.7%	300 W Xenon lamp	particle	hydrothermal method	20
CuFe ₂ O ₄ /g-C ₃ N ₄	103.7	1	120	propranolol (PRO)	82.2%	350W Xenon lamp; $\lambda > 420$ nm	layered structure	sol-gel combustion method	21
Ag ₃ PO ₄ /NrGO/CuFe ₂ O ₄	15	0.3	60	2,4-dichlorophenol (2,4-DCP)	95.3%	Xe lamp 250 W; $\lambda \leq 420$ nm	tetrahedronnano particles morphology	Coprecipitation method	22
Bi ₂ Te ₃ /CdS/CuFe ₂ O ₄	40	1.4	180	Methylene Blue (MB)	97.15%	ungsten-halogen lamp	Nanorod with anoparticles	wet impregnation method	23
CuFe ₂ O ₄ /C	20	0.6	60	rhodamine B (RhB)	99.1%	350W Xenon lamp	Hollow nanospheres	one pot synthetic calcination method	This work

References

- Xiang, Y.; Huang, Y.; Xiao, B.; Wu, X.; Zhang, G. Magnetic yolk-shell structure of ZnFe₂O₄ nanoparticles for enhanced visible light photo-Fenton degradation towards antibiotics and mechanism study. *Appl. Surf. Sci.* **2020**, *513*, 145820.
- Wang, Y.; Song, H.; Chen, J.; Chai, S.; Chen, C.; Wang, Y.; He, C. A novel solar photo-Fenton system with self-synthesizing H₂O₂: Enhanced photo-induced catalytic performances and mechanism insights. *Appl. Surf. Sci.* **2020**, *512*, 145650.
- Han, C.; Park, H. D.; Kim, S.B.; Yargeau, V.V.; Choi, J. W.; Lee, S. H.; Park, J. A. Oxidation of tetracycline and oxytetracycline for the photo-Fenton process: Their transformation products and toxicity assessment. *Water Res.* **2020**, *172*, 115514.
- Huang, S.; Zhang, Q.; Liu, P.; Ma, S.; Xie, B.; Yang, K.; Zhao, Y. Novel up-conversion carbon quantum dots/ α -FeOOH nanohybrids eliminate tetracycline and its related drug resistance in visible-light responsive Fenton system. *Appl. Catal. B-Environ.* **2020**, *263*, 118336.
- Wu, Q.; Yang, H.; Kang, L.; Gao, Z.; Ren, F. Appl. Catal. Fe-based metal-organic frameworks as Fenton-like catalysts for highly efficient degradation of tetracycline hydrochloride over a wide pH range: acceleration of Fe(II)/Fe(III) cycle under visible light irradiation. *B-Environ.* **2020**, *263*, 118282.

6. Zhao, J.; Ji, M.; Di, J.; Zhang, Y.; He, M.; Li, H.; Xia, J. Novel Z-scheme heterogeneous photo-Fenton-like g-C₃N₄/FeOCl for the pollutants degradation under visible light irradiation. *J. Photochem. Photobiol., A* **2020**, *391*, 112343.
7. Guo, L.; Zhang, K.; Han, X.; Zhao, Q.; Wang, D.; Fu, F.; Liang, Y. Highly efficient visible-light-driven photo-Fenton catalytic performance over FeOOH/Bi₂WO₆ composite for organic pollutant degradation. *Alloys. Compds.* **2020**, *816*, 152560.
8. Li, X.; Zeng, Z.; Zeng, G.; Wang, D.; Xiao, R.; Wang, Y.; Zhou, C.; Yi, H.; Ye, S.; Yang, Y.; et al. A “bottle-around-ship” like method synthesized yolk-shell Ag₃PO₄@MIL-53(Fe) Z-scheme photocatalysts for enhanced tetracycline removal. *J. Colloid Interface Sci.* **2020**, *561*, 501–511.
9. Jiang, J.; Gao, J.; Li, T.; Chen, Y.; Wu, Q.; Xie, T.; Lin, Y.; Dong, S. Visible-light-driven photo-Fenton reaction with α-Fe₂O₃/BiOI at near neutral pH: Boosted photogenerated charge separation, optimum operating parameters and mechanism insight. *J. Colloid Interface Sci.* **2019**, *554*, 531–543.
10. Qi, Y.; Mei, Y.; Li, J.; Yao, T.; Yang, Y.; Jia, W.; Tong, X.; Wu, J.; Xin, B. Highly efficient microwave-assisted Fenton degradation of tetracycline using pine-needle-like CuCo₂O₄ nanocatalyst. *Chem. Eng. J.* **2019**, *373*, 1158–1167.
11. Zhu, G.; Yu, X.; Xie, F.; Feng, W. Ultraviolet light assisted heterogeneous Fenton degradation of tetracycline based on polyhedral Fe₃O₄ nanoparticles with exposed high-energy {110} facets. *Appl. Surf. Sci.* **2019**, *485*, 496–505.
12. Guo, L.; Zhang, K.; Han, X.; Zhao, Q.; Wang, D.; Fu, F. 2D In-Plane CuS/Bi₂WO₆ p-n heterostructures with promoted visible-light-driven Photo-Fenton degradation performance. *Nanomater.* **2019**, *8*, 1151.
13. Lai, C.; Huang, F.; Zeng, G.; Huang, D.; Qin, L.; Cheng, M.; Zhang, C.; Li, B.; Yi, H.; Liu, S.; et al. Fabrication of novel magnetic MnFe₂O₄/bio-char composite and heterogeneous photo-Fenton degradation of tetracycline in near neutral pH. *Chemosphere.* **2019**, *224*, 910–921.
14. Chen, Z.; Gao, Y.; Mu, D.; Shi, H.; Lou, D.; Liu, S. Recyclable magnetic NiFe₂O₄/C yolk-shell nanospheres with excellent visible-light-Fenton degradation performance of tetracycline hydrochloride. *Dalton Trans.* **2019**, *48*, 3038–3044.
15. Zheng, X.; Fu, W.; Kang, F.; Peng, H.; Wen, J. Enhanced photo-Fenton degradation of tetracycline using TiO₂-coated α-Fe₂O₃ core-shell heterojunction. *J. Ind. Eng. Chem.* **2018**, *68*, 14–23.
16. Du, D.; Shi, W.; Wang, L.; Zhang, J. Yolk-shell structured Fe₃O₄@void@TiO₂ as a photo-Fenton-like catalyst for the extremely efficient elimination of tetracycline. *Appl. Catal., B.* **2017**, *200*, 484–492.
17. Dong, Z.; Niu, C.; Guo, H.; Niu, H.; Liang, S.; Liang, C.; Liu, H.; Yang, Y. Anchoring CuFe₂O₄ nanoparticles into N-doped carbon nanosheets for peroxymonosulfate activation: Built-in electric field dominated radical and non-radical process. *Chem. Eng. J.* **2021**, *426*, 130850.
18. Shetty, K.; Renuka, L.; Nagaswarupa, H.; Nagabhushana, H.; Anantharaju, K.; Rangappa, D.; Prashantha, S.; Ashwini, K. A comparative study on CuFe₂O₄, ZnFe₂O₄ and NiFe₂O₄: Morphology, Impedance and Photocatalytic studies. *Mater. Today: Proc.* **2017**, *4*, 11806–11815.
19. Sun, Q.; Wang, X.; Liu, Y.; Xia, S.; Zhao, J. Activation of peroxymonosulfate by a floating oxygen vacancies - CuFe₂O₄ photocatalyst under visible light for efficient degradation of sulfamethazine. *Sci. Total Environ.* **2022**, *824*, 153630.
20. Zhang, X.; Zhao, Y. Optimization of photocatalytic degradation of dye wastewater by CuFe₂O₄/AgBr composite using response surface methodology. *Mater. Res. Express.* **2018**, *6*, 036109.
21. Li, R.; Cai, M.; Xie, Z.; Zhang, Q.; Zeng, Y.; Liu, H.; Liu, G.; Lv, W. Construction of heterostructured CuFe₂O₄/g-C₃N₄ nanocomposite as an efficient visible light photocatalyst with peroxydisulfate for the organic oxidation. *Appl. Catal., B.* **2019**, *244*, 974–982.
22. Wei, X.; Yang, X.; Xu, X.; Liu, Z.; Naraginti, S.; Wan, J. Novel magnetically separable tetrahedral Ag₃PO₄/NrGO/CuFe₂O₄ photocatalyst for efficient detoxification of 2,4-dichlorophenol. *Environ. Res.* **2021**, *201*, 111519.
23. Palanisamy, G.; Bhuvaneshwari, K.; Bharathi, G.; Pazhanivel, T.; Dhanalakshmi, M. Improved photocatalytic performance of magnetically recoverable Bi₂Te₃/CdS/CuFe₂O₄ nanocomposite for MB dye under visible light exposure. *Solid State Sci.* **2021**, *115*, 106584.